

# Centrality and transverse momentum dependence of elliptic flow of multi-strange hadrons and $\phi$ meson in Au+Au collisions at $\sqrt{s_{NN}} = 200$ GeV

L. Adamczyk<sup>1</sup>, J. K. Adkins<sup>20</sup>, G. Agakishiev<sup>18</sup>, M. M. Aggarwal<sup>30</sup>, Z. Ahammed<sup>47</sup>, I. Alekseev<sup>16</sup>, A. Aparin<sup>18</sup>, D. Arkhipkin<sup>3</sup>, E. C. Aschenauer<sup>3</sup>, G. S. Averichev<sup>18</sup>, V. Bairathi<sup>27</sup>, A. Banerjee<sup>47</sup>, R. Bellwied<sup>43</sup>, A. Bhasin<sup>17</sup>, A. K. Bhati<sup>30</sup>, P. Bhattarai<sup>42</sup>, J. Bielcik<sup>10</sup>, J. Bielcikova<sup>11</sup>, L. C. Bland<sup>3</sup>, I. G. Bordyuzhin<sup>16</sup>, J. Bouchet<sup>19</sup>, A. V. Brandin<sup>26</sup>, I. Bunzarov<sup>18</sup>, J. Butterworth<sup>36</sup>, H. Caines<sup>51</sup>, M. Calderón de la Barca Sánchez<sup>5</sup>, J. M. Campbell<sup>28</sup>, D. Cebra<sup>5</sup>, M. C. Cervantes<sup>41</sup>, I. Chakaberia<sup>3</sup>, P. Chaloupka<sup>10</sup>, Z. Chang<sup>41</sup>, S. Chattopadhyay<sup>47</sup>, J. H. Chen<sup>39</sup>, X. Chen<sup>22</sup>, J. Cheng<sup>44</sup>, M. Cherney<sup>9</sup>, W. Christie<sup>3</sup>, G. Contin<sup>23</sup>, H. J. Crawford<sup>4</sup>, S. Das<sup>13</sup>, L. C. De Silva<sup>9</sup>, R. R. Debbé<sup>3</sup>, T. G. Dedovich<sup>18</sup>, J. Deng<sup>38</sup>, A. A. Derevschikov<sup>32</sup>, B. di Ruzza<sup>3</sup>, L. Didenko<sup>3</sup>, C. Dilks<sup>31</sup>, X. Dong<sup>23</sup>, J. L. Drachenberg<sup>46</sup>, J. E. Draper<sup>5</sup>, C. M. Du<sup>22</sup>, L. E. Dunkelberger<sup>6</sup>, J. C. Dunlop<sup>3</sup>, L. G. Efimov<sup>18</sup>, J. Engelage<sup>4</sup>, G. Eppley<sup>36</sup>, R. Esha<sup>6</sup>, O. Evdokimov<sup>8</sup>, O. Eyser<sup>3</sup>, R. Fatemi<sup>20</sup>, S. Fazio<sup>3</sup>, P. Federic<sup>11</sup>, J. Fedorisin<sup>18</sup>, Z. Feng<sup>7</sup>, P. Filip<sup>18</sup>, Y. Fisyak<sup>3</sup>, C. E. Flores<sup>5</sup>, L. Fulek<sup>1</sup>, C. A. Gagliardi<sup>41</sup>, D. Garand<sup>33</sup>, F. Geurts<sup>36</sup>, A. Gibson<sup>46</sup>, M. Girard<sup>48</sup>, L. Greiner<sup>23</sup>, D. Grosnick<sup>46</sup>, D. S. Gunarathne<sup>40</sup>, Y. Guo<sup>37</sup>, S. Gupta<sup>17</sup>, A. Gupta<sup>17</sup>, W. Guryn<sup>3</sup>, A. Hamad<sup>19</sup>, A. Hamed<sup>41</sup>, R. Haque<sup>27</sup>, J. W. Harris<sup>51</sup>, L. He<sup>33</sup>, S. Heppelmann<sup>3</sup>, S. Heppelmann<sup>31</sup>, A. Hirsch<sup>33</sup>, G. W. Hoffmann<sup>42</sup>, D. J. Hofman<sup>8</sup>, S. Horvat<sup>51</sup>, X. Huang<sup>44</sup>, B. Huang<sup>8</sup>, H. Z. Huang<sup>6</sup>, P. Huck<sup>7</sup>, T. J. Humanic<sup>28</sup>, G. Igo<sup>6</sup>, W. W. Jacobs<sup>15</sup>, H. Jang<sup>21</sup>, K. Jiang<sup>37</sup>, E. G. Judd<sup>4</sup>, S. Kabana<sup>19</sup>, D. Kalinkin<sup>16</sup>, K. Kang<sup>44</sup>, K. Kauder<sup>49</sup>, H. W. Ke<sup>3</sup>, D. Keane<sup>19</sup>, A. Kechechyan<sup>18</sup>, Z. H. Khan<sup>8</sup>, D. P. Kikoła<sup>48</sup>, I. Kisel<sup>12</sup>, A. Kisel<sup>48</sup>, L. Kochenda<sup>26</sup>, D. D. Koetke<sup>46</sup>, T. Kollegger<sup>12</sup>, L. K. Kosarzewski<sup>48</sup>, A. F. Kraishan<sup>40</sup>, P. Kravtsov<sup>26</sup>, K. Krueger<sup>2</sup>, I. Kulakov<sup>12</sup>, L. Kumar<sup>30</sup>, R. A. Kycia<sup>29</sup>, M. A. C. Lamont<sup>3</sup>, J. M. Landgraf<sup>3</sup>, K. D. Landry<sup>6</sup>, J. Lauret<sup>3</sup>, A. Lebedev<sup>3</sup>, R. Lednicky<sup>18</sup>, J. H. Lee<sup>3</sup>, Z. M. Li<sup>7</sup>, W. Li<sup>39</sup>, X. Li<sup>3</sup>, X. Li<sup>40</sup>, C. Li<sup>37</sup>, Y. Li<sup>44</sup>, M. A. Lisa<sup>28</sup>, F. Liu<sup>7</sup>, T. Ljubicic<sup>3</sup>, W. J. Llope<sup>49</sup>, M. Lomnitz<sup>19</sup>, R. S. Longacre<sup>3</sup>, X. Luo<sup>7</sup>, Y. G. Ma<sup>39</sup>, G. L. Ma<sup>39</sup>, L. Ma<sup>39</sup>, R. Ma<sup>3</sup>, N. Magdy<sup>50</sup>, R. Majka<sup>51</sup>, A. Manion<sup>23</sup>, S. Margetis<sup>19</sup>, C. Markert<sup>42</sup>, H. Masui<sup>23</sup>, H. S. Matis<sup>23</sup>, D. McDonald<sup>43</sup>, K. Meehan<sup>5</sup>, N. G. Minaev<sup>32</sup>, S. Mioduszewski<sup>41</sup>, D. Mishra<sup>27</sup>, B. Mohanty<sup>27</sup>, M. M. Mondal<sup>41</sup>, D. A. Morozov<sup>32</sup>, M. K. Mustafa<sup>23</sup>, B. K. Nandi<sup>14</sup>, Md. Nasim<sup>6</sup>, T. K. Nayak<sup>47</sup>, G. Nigmatkulov<sup>26</sup>, L. V. Nogach<sup>32</sup>, S. Y. Noh<sup>21</sup>, J. Novak<sup>25</sup>, S. B. Nurushev<sup>32</sup>, G. Odyniec<sup>23</sup>, A. Ogawa<sup>3</sup>, K. Oh<sup>34</sup>, V. Okorokov<sup>26</sup>, D. Olivitt Jr.<sup>40</sup>, B. S. Page<sup>3</sup>, R. Pak<sup>3</sup>, Y. X. Pan<sup>6</sup>, Y. Pandit<sup>8</sup>, Y. Panebratsev<sup>18</sup>, B. Pawlik<sup>29</sup>, H. Pei<sup>7</sup>, C. Perkins<sup>4</sup>, A. Peterson<sup>28</sup>, P. Pile<sup>3</sup>, M. Planinic<sup>52</sup>, J. Pluta<sup>48</sup>, N. Poljak<sup>52</sup>, K. Poniatowska<sup>48</sup>, J. Porter<sup>23</sup>, M. Posik<sup>40</sup>, A. M. Poskanzer<sup>23</sup>, J. Putschke<sup>49</sup>, H. Qiu<sup>23</sup>, A. Quintero<sup>19</sup>, S. Ramachandran<sup>20</sup>, R. Raniwala<sup>35</sup>, S. Raniwala<sup>35</sup>, R. L. Ray<sup>42</sup>, H. G. Ritter<sup>23</sup>, J. B. Roberts<sup>36</sup>, O. V. Rogachevskiy<sup>18</sup>, J. L. Romero<sup>5</sup>, A. Roy<sup>47</sup>, L. Ruan<sup>3</sup>, J. Rusnak<sup>11</sup>, O. Rusnakova<sup>10</sup>, N. R. Sahoo<sup>41</sup>, P. K. Sahu<sup>13</sup>, I. Sakrejda<sup>23</sup>, S. Salur<sup>23</sup>, J. Sandweiss<sup>51</sup>, A. Sarkar<sup>14</sup>, J. Schambach<sup>42</sup>, R. P. Scharenberg<sup>33</sup>, A. M. Schmah<sup>23</sup>, W. B. Schmidke<sup>3</sup>, N. Schmitz<sup>24</sup>, J. Seger<sup>9</sup>, P. Seyboth<sup>24</sup>, N. Shah<sup>39</sup>, E. Shahaiev<sup>18</sup>, P. V. Shanmuganathan<sup>19</sup>, M. Shao<sup>37</sup>, B. Sharma<sup>30</sup>, M. K. Sharma<sup>17</sup>, W. Q. Shen<sup>39</sup>, S. S. Shi<sup>7</sup>, Q. Y. Shou<sup>39</sup>, E. P. Sichtermann<sup>23</sup>, R. Sikora<sup>1</sup>, M. Simko<sup>11</sup>, S. Singha<sup>19</sup>, M. J. Skoby<sup>15</sup>, D. Smirnov<sup>3</sup>, N. Smirnov<sup>51</sup>, L. Song<sup>43</sup>, P. Sorensen<sup>3</sup>, H. M. Spinka<sup>2</sup>, B. Srivastava<sup>33</sup>, T. D. S. Stanislaus<sup>46</sup>, M. Stepanov<sup>33</sup>, R. Stock<sup>12</sup>, M. Strikhanov<sup>26</sup>, B. Stringfellow<sup>33</sup>, M. Sumera<sup>11</sup>, B. Summa<sup>31</sup>, X. Sun<sup>23</sup>, X. M. Sun<sup>7</sup>, Y. Sun<sup>37</sup>, Z. Sun<sup>22</sup>, B. Surrow<sup>40</sup>, N. Svirida<sup>16</sup>, M. A. Szelezniak<sup>23</sup>, A. H. Tang<sup>3</sup>, Z. Tang<sup>37</sup>, T. Tarnowsky<sup>25</sup>, A. Tawfik<sup>50</sup>, J. H. Thomas<sup>23</sup>, A. R. Timmins<sup>43</sup>, D. Tlusty<sup>11</sup>, M. Tokarev<sup>18</sup>, S. Trentalange<sup>6</sup>, R. E. Tribble<sup>41</sup>, P. Tribedy<sup>47</sup>, S. K. Tripathy<sup>13</sup>, B. A. Trzeciak<sup>10</sup>, O. D. Tsai<sup>6</sup>, T. Ullrich<sup>3</sup>, D. G. Underwood<sup>2</sup>, I. Upsal<sup>28</sup>, G. Van Buren<sup>3</sup>, G. van Nieuwenhuizen<sup>3</sup>, M. Vandenbroucke<sup>40</sup>, R. Varma<sup>14</sup>, A. N. Vasiliev<sup>32</sup>, R. Vertesi<sup>11</sup>, F. Videbæk<sup>3</sup>, Y. P. Viyogi<sup>47</sup>, S. Vokal<sup>18</sup>, S. A. Voloshin<sup>49</sup>, A. Vossen<sup>15</sup>, Y. Wang<sup>44</sup>, G. Wang<sup>6</sup>, J. S. Wang<sup>22</sup>, H. Wang<sup>3</sup>, Y. Wang<sup>7</sup>, F. Wang<sup>33</sup>, J. C. Webb<sup>3</sup>, G. Webb<sup>3</sup>, L. Wen<sup>6</sup>, G. D. Westfall<sup>25</sup>, H. Wieman<sup>23</sup>, S. W. Wissink<sup>15</sup>, R. Witt<sup>45</sup>, Y. F. Wu<sup>7</sup>, Y. Wu<sup>19</sup>, Z. G. Xiao<sup>44</sup>, W. Xie<sup>33</sup>, K. Xin<sup>36</sup>, N. Xu<sup>23</sup>, Z. Xu<sup>3</sup>, Q. H. Xu<sup>38</sup>, Y. F. Xu<sup>39</sup>, H. Xu<sup>22</sup>, Q. Yang<sup>37</sup>, Y. Yang<sup>7</sup>, Y. Yang<sup>22</sup>, S. Yang<sup>37</sup>, C. Yang<sup>37</sup>, Z. Ye<sup>8</sup>, P. Yepes<sup>36</sup>, L. Yi<sup>51</sup>, K. Yip<sup>3</sup>, I. -K. Yoo<sup>34</sup>, N. Yu<sup>7</sup>, H. Zbroszczyk<sup>48</sup>, W. Zha<sup>37</sup>, Z. Zhang<sup>39</sup>, Y. Zhang<sup>37</sup>, J. B. Zhang<sup>7</sup>, J. Zhang<sup>38</sup>, S. Zhang<sup>39</sup>, J. Zhang<sup>22</sup>, X. P. Zhang<sup>44</sup>, J. Zhao<sup>7</sup>, C. Zhong<sup>39</sup>, L. Zhou<sup>37</sup>, X. Zhu<sup>44</sup>, Y. Zoulkarneeva<sup>18</sup>, M. Zyzak<sup>12</sup>

<sup>1</sup>AGH University of Science and Technology, Cracow 30-059, Poland

<sup>2</sup>Argonne National Laboratory, Argonne, Illinois 60439, USA

<sup>3</sup>Brookhaven National Laboratory, Upton, New York 11973, USA

<sup>4</sup>University of California, Berkeley, California 94720, USA

<sup>5</sup>University of California, Davis, California 95616, USA

<sup>6</sup>University of California, Los Angeles, California 90095, USA

<sup>7</sup>Central China Normal University (HZNU), Wuhan 430079, China

<sup>8</sup>University of Illinois at Chicago, Chicago, Illinois 60607, USA

<sup>9</sup>Creighton University, Omaha, Nebraska 68178, USA

- <sup>10</sup> Czech Technical University in Prague, FNSPE, Prague, 115 19, Czech Republic  
<sup>11</sup> Nuclear Physics Institute AS CR, 250 68 Řež/Prague, Czech Republic  
<sup>12</sup> Frankfurt Institute for Advanced Studies FIAS, Frankfurt 60438, Germany  
<sup>13</sup> Institute of Physics, Bhubaneswar 751005, India  
<sup>14</sup> Indian Institute of Technology, Mumbai 400076, India  
<sup>15</sup> Indiana University, Bloomington, Indiana 47408, USA  
<sup>16</sup> Alikhanov Institute for Theoretical and Experimental Physics, Moscow 117218, Russia  
<sup>17</sup> University of Jammu, Jammu 180001, India  
<sup>18</sup> Joint Institute for Nuclear Research, Dubna, 141 980, Russia  
<sup>19</sup> Kent State University, Kent, Ohio 44242, USA  
<sup>20</sup> University of Kentucky, Lexington, Kentucky, 40506-0055, USA  
<sup>21</sup> Korea Institute of Science and Technology Information, Daejeon 305-701, Korea  
<sup>22</sup> Institute of Modern Physics, Lanzhou 730000, China  
<sup>23</sup> Lawrence Berkeley National Laboratory, Berkeley, California 94720, USA  
<sup>24</sup> Max-Planck-Institut für Physik, Munich 80805, Germany  
<sup>25</sup> Michigan State University, East Lansing, Michigan 48824, USA  
<sup>26</sup> Moscow Engineering Physics Institute, Moscow 115409, Russia  
<sup>27</sup> National Institute of Science Education and Research, Jatni 752050, Odisha, India  
<sup>28</sup> Ohio State University, Columbus, Ohio 43210, USA  
<sup>29</sup> Institute of Nuclear Physics PAN, Cracow 31-342, Poland  
<sup>30</sup> Panjab University, Chandigarh 160014, India  
<sup>31</sup> Pennsylvania State University, University Park, Pennsylvania 16802, USA  
<sup>32</sup> Institute of High Energy Physics, Protvino 142281, Russia  
<sup>33</sup> Purdue University, West Lafayette, Indiana 47907, USA  
<sup>34</sup> Pusan National University, Pusan 609735, Republic of Korea  
<sup>35</sup> University of Rajasthan, Jaipur 302004, India  
<sup>36</sup> Rice University, Houston, Texas 77251, USA  
<sup>37</sup> University of Science and Technology of China, Hefei 230026, China  
<sup>38</sup> Shandong University, Jinan, Shandong 250100, China  
<sup>39</sup> Shanghai Institute of Applied Physics, Shanghai 201800, China  
<sup>40</sup> Temple University, Philadelphia, Pennsylvania 19122, USA  
<sup>41</sup> Texas A&M University, College Station, Texas 77843, USA  
<sup>42</sup> University of Texas, Austin, Texas 78712, USA  
<sup>43</sup> University of Houston, Houston, Texas 77204, USA  
<sup>44</sup> Tsinghua University, Beijing 100084, China  
<sup>45</sup> United States Naval Academy, Annapolis, Maryland, 21402, USA  
<sup>46</sup> Valparaiso University, Valparaiso, Indiana 46383, USA  
<sup>47</sup> Variable Energy Cyclotron Centre, Kolkata 700064, India  
<sup>48</sup> Warsaw University of Technology, Warsaw 00-661, Poland  
<sup>49</sup> Wayne State University, Detroit, Michigan 48201, USA  
<sup>50</sup> World Laboratory for Cosmology and Particle Physics (WLCAPP), Cairo 11571, Egypt  
<sup>51</sup> Yale University, New Haven, Connecticut 06520, USA and  
<sup>52</sup> University of Zagreb, Zagreb, HR-10002, Croatia
- (STAR Collaboration)

We present high precision measurements of elliptic flow near midrapidity ( $|y| < 1.0$ ) for multi-strange hadrons and  $\phi$  meson as a function of centrality and transverse momentum in Au+Au collisions at center of mass energy  $\sqrt{s_{NN}} = 200$  GeV. We observe that the transverse momentum dependence of  $\phi$  and  $\Omega$   $v_2$  is similar to that of  $\pi$  and  $p$ , respectively, which may indicate that the heavier strange quark flows as strongly as the lighter up and down quarks. This observation constitutes a clear piece of evidence for the development of partonic collectivity in heavy-ion collisions at the top RHIC energy. Number of constituent quark scaling is found to hold within statistical uncertainty for both 0-30% and 30-80% collision centrality. There is an indication of the breakdown of previously observed mass ordering between  $\phi$  and proton  $v_2$  at low transverse momentum in the 0-30% centrality range, possibly indicating late hadronic interactions affecting the proton  $v_2$ .

At sufficiently high temperature and/or high density Quantum Chromodynamics (QCD) predicts a transition from hadronic matter to de-confined partonic matter [1]. The main goal of the STAR (Solenoid Tracker at RHIC) experiment at the Relativistic Heavy Ion Collider (RHIC) is to study the properties of QCD matter at

extremely high energy and parton densities, created in the heavy-ion collision. In high energy heavy-ion collisions, particles are produced with an azimuthally anisotropic momentum distribution, which is a result of hydrodynamical flow of the Quark-Gluon-Plasma (in the soft regime). One way to examine this anisotropy is to

measure elliptic flow ( $v_2$ ), which plays a crucial role in the study of the QCD matter formed during the collision. The elliptic flow, defined as  $v_2 = \langle \cos 2(\varphi - \Psi) \rangle$ , is the second Fourier coefficient of the azimuthal distribution of the emitted particle with respect to the reaction plane (defined by the beam axis and a vector between the centers of the colliding ions). Here  $\varphi$  is the azimuthal angle of emitted particle and  $\Psi$  is the azimuthal angle of the reaction plane. Over the past decade, experimental measurements have shown elliptic flow to be especially sensitive to the initial phase and equation of state of the system formed in heavy-ion collisions [2–6]. However, information about the early dynamics of the system may be modified by hadronic re-scattering in the later stage of the collision [7, 8]. The hadronic interaction cross-sections of  $\phi$ ,  $\Xi$  and  $\Omega$  are expected to be small [9] and their freeze-out temperatures are close to the quark-hadron transition temperature predicted by lattice QCD [10, 11]. Hence, these hadrons are expected to provide information primarily from the partonic stage of the collision [12–16]. Previous measurements of  $\phi$  and  $\Omega$   $v_2$  from STAR [17] were statistically limited and little is known about the centrality dependence of  $\Omega$   $v_2$ . The measurements of  $\phi$  and  $\Omega$   $v_2$  presented here as a function of both transverse momentum ( $p_T$ ) and centrality help to alleviate these limitations. Moreover, high precision measurements of  $\phi$ -meson  $v_2$  relative to proton  $v_2$  at low  $p_T$  may provide information on the effect of hadronic re-scattering [7, 8] in the late stages of the collision.

We present the collision centrality and  $p_T$  dependence of the elliptic flow of  $\pi^+ + \pi^-$ ,  $K^+ + K^-$ ,  $K_S^0$ ,  $p + \bar{p}$ ,  $\phi$ ,  $\Lambda + \bar{\Lambda}$ ,  $\Xi^- + \Xi^+$  and  $\Omega^- + \bar{\Omega}^+$ . For this study we used 730 million of Au+Au events at  $\sqrt{s_{NN}} = 200$  GeV recorded by STAR in 2010 and 2011 with a minimum-bias trigger [18]. The collision centrality is determined by comparing the measured raw charged hadron multiplicity from the Time Projection Chamber (TPC) within a pseudorapidity window  $|\eta| < 0.5$  with Glauber Monte-Carlo simulations [19, 20]. The TPC and Time of Flight (TOF) detectors with full azimuthal coverage are used for particle identification in the central rapidity region ( $|\eta| < 1.0$  for TPC and  $|\eta| < 0.9$  for TOF). Charged particles are identified using specific ionization energy loss as a function of momentum (in the TPC) and square of the particle mass as a function of momentum (for the TOF). We reconstruct short-lived  $K_S^0$ ,  $\Lambda$ ,  $\Xi$ ,  $\Omega$  and  $\phi$  through the following decay channels:  $K_S^0 \rightarrow \pi^+ + \pi^-$ ,  $\Lambda \rightarrow p + \pi$ ,  $\Xi \rightarrow \Lambda + \pi$ ,  $\Omega \rightarrow \Lambda + K$  and  $\phi \rightarrow K^+ + K^-$ . Topological and kinematic cuts are applied to reduce the combinatorial background for  $K_S^0$ ,  $\Lambda$ ,  $\Xi$  and  $\Omega$ . The detailed description of the procedures can be found in Refs. [17, 21, 22].

The  $\eta$  sub-event plane method [23] is used for the elliptic flow analysis. An  $\eta$  gap of  $|\Delta\eta| > 0.1$  between positive and negative pseudorapidity sub-events is introduced to suppress non-flow effects. The  $v_2$  for short-lived hadrons ( $K_S^0$ ,  $\phi$ ,  $\Lambda$ ,  $\Xi$  and  $\Omega$ ) is calculated as a function of invariant mass for each  $p_T$  and centrality bin in order

to take into account the invariant mass dependence of the signal to background ratio. Details of this method can be found in Ref. [24]. The observed  $v_2$  values are corrected for finite event plane resolution which is determined by comparing the two  $\eta$ -sub event plane angles. A resolution correction is done by dividing the term  $\cos 2(\varphi - \Psi_2)$  by the event plane resolution for the corresponding centrality for each event following the method described in Refs. [25, 26]. The change in  $v_2$  between present method of resolution correction and the previous method used in earlier STAR publication [4–6] is  $\leq 5\%$  at  $\sqrt{s_{NN}} = 200$  GeV. Here  $\Psi_2$  is the 2<sup>nd</sup> order event plane which is used for  $v_2$  measurements.

For all particle species, the cuts used for particle identification (PID) and background subtraction are varied to estimate the systematic errors. Furthermore, different techniques (e.g. by counting entries in each bin of the invariant mass histogram or by fitting the shape of the invariant mass distribution using a function) for yield extraction are used. For  $\pi^\pm$ ,  $K^\pm$  and  $p(\bar{p})$ , 6 different combinations of track cuts and 3 different sets of PID cuts which finally yield 18 combinations have been used. For other strange hadrons ( $K_S^0$ ,  $\phi$ ,  $\Lambda$ ,  $\Xi$  and  $\Omega$ ) 20 different cut combination are used. The root-mean-square value of point-by-point difference from the default value ( $v_2$  from default set of cuts) is used as the systematic error on each data point. The total systematic error depends on  $p_T$ , centrality and particle species. We observed 3-5% systematic error for  $p_T < 1.5$  GeV/c and 0-30% centrality for  $\phi$ ,  $K_S^0$ ,  $\Lambda$  whereas for  $\Xi$  and  $\Omega$  the systematic error varies from 8% to 14%. Total systematic errors are less than 1% for  $\pi^\pm$ ,  $K^\pm$  and  $p(\bar{p})$  for all  $p_T$  and centralities.

We investigated the effect of track reconstruction efficiency on the measured  $v_2$  of identified hadrons for wide centrality bins, such as a 0-80% centrality bin. The centrality dependence of track reconstruction efficiency biases the measured  $v_2$  toward events with higher reconstruction efficiency, an effect we will refer to as an “efficiency bias”. Due to the efficiency bias, the  $v_2$  of  $\Xi$  and  $\Omega$ , each having three daughters, changes by no more than 5% in 0-80% centrality. For the other measured particles, the effect is less than 3% for 0-80% centrality. The  $v_2(p_T)$  of all particles presented here have been corrected for the efficiency bias by using the inverse of efficiency as a weight for the  $v_2$  as a function of  $p_T$  and centrality.

An additional correction is needed for  $\phi$ ,  $\Xi$  and  $\Omega$   $v_2$ . An event bias is naturally introduced when one measures  $v_2$  in wide centrality bins, especially for the rare particles. As the measured  $v_2$  is an average over all events weighted by particle yield, the average event shape depends on the particle type. A Glauber model [19] study of the average initial participant eccentricity indicates the multi-strange hadron  $v_2$  is more biased toward central events than that of the light and strange hadrons. Specifically, the average eccentricity for multi-strange hadrons in wide centrality bins is

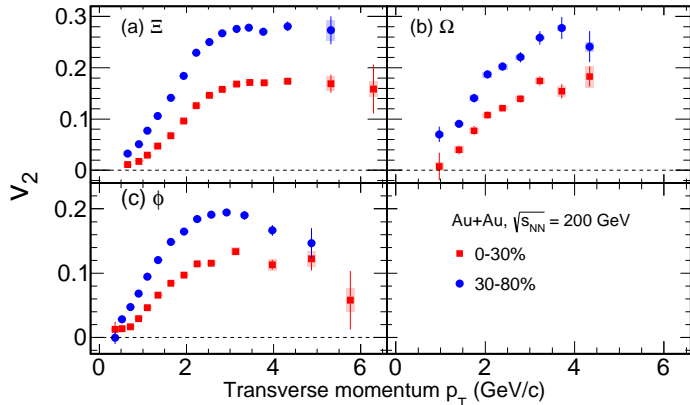


FIG. 1. (Color online) The  $v_2$  as a function of  $p_T$  near midrapidity ( $|y| < 1.0$ ) for (a)  $\Xi^- + \Xi^+$  (b)  $\Omega^- + \Omega^+$  and (c)  $\phi$  from Au + Au collisions at  $\sqrt{s_{NN}} = 200$  GeV for 0-30% and 30-80% centrality. The systematic uncertainties are shown by shaded boxes and the statistical uncertainties by vertical lines.

smaller than the eccentricity determined by the particle yield of all charged hadrons. One should take this effect into consideration if any conclusion on the number of constituent quark scaling is drawn. This bias can be corrected by normalizing the measured  $v_2$  by the ratio of eccentricity to that weighted by the yield of the particle of interest. We find the event bias correction factors for 0-30%, 30-80%, and 0-80% centralities are 1.002, 1.053 and 1.028 for  $\phi$ ; 1.019, 1.054 and 1.091 for  $\Xi$ ; 1.068, 1.067 and 1.177 for  $\Omega$ . The event bias correction for light and strange hadrons is small ( $< 0.03$ ), perhaps be due to their copious production. Therefore, in the later discussion of number of constituent quark (NCQ) scaling, the event bias correction is applied only to the  $v_2$  of multi-strange hadrons and  $\phi$  meson. The above correction factors remain almost unchanged if we use Color-Glass Condensate (CGC) [27] based model to calculate eccentricity.

In Figure 1 we present the elliptic flow parameter  $v_2(p_T)$  at midrapidity ( $|y| < 1.0$ ) for (a)  $\Xi^- + \Xi^+$ , (b)  $\Omega^- + \Omega^+$  and (c)  $\phi$  in Au + Au collisions at  $\sqrt{s_{NN}} = 200$  GeV for 0-30% and 30-80% centrality. Event bias correction factors have been applied to the results shown in Fig 1. A clear centrality dependence of  $v_2(p_T)$  is observed for  $\phi$ ,  $\Xi$  and  $\Omega$ , similar to that of identified light and strange hadrons previously measured by the STAR experiment [28]. The values of  $v_2$  are found to be larger in peripheral collisions (30-80% centrality) compared to those in central collisions (0-30% centrality). This observation is consistent with an interpretation in which the final momentum anisotropy is driven by the initial spatial anisotropy.

The NCQ scaling in  $v_2$  for different identified hadrons is considered to be a good probe for studying the strongly

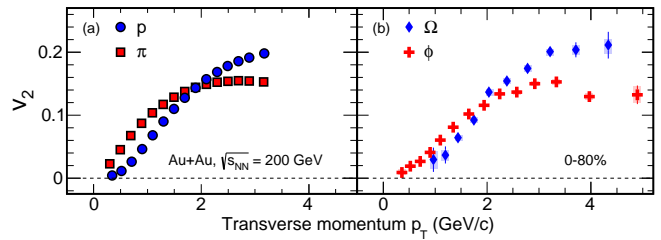


FIG. 2. (Color online) The  $v_2$  as function of  $p_T$  for  $\pi$ ,  $p$  (panel a) and  $\phi$ ,  $\Omega$  (panel b) from minimum bias Au+Au collisions at  $\sqrt{s_{NN}} = 200$  GeV for 0-80% centrality. The systematic uncertainties are shown by the shaded boxes while vertical lines represent the statistical uncertainties.

interacting partonic matter. The observed NCQ scaling of identified hadrons in experimental data [29] indicates the importance of parton recombination in forming hadrons in the intermediate  $p_T$  range ( $2.0 \text{ GeV}/c < p_T < 4.0 \text{ GeV}/c$ ) [30–33]. Such scaling may indicate that collective elliptic flow develops during the partonic phase. Previous measurements have found that  $v_2$  of  $\pi$ ,  $K$ ,  $p$ ,  $K_S^0$ ,  $\Lambda$ ,  $\Xi$  and  $\phi$  follow NCQ scaling well at top the RHIC energy ( $\sqrt{s_{NN}} = 200$  GeV) [29]. The large statistics data sets collected by STAR detectors allow us to measure elliptic flow of multi-strange hadrons, specifically that of the  $\Omega$  baryon which is made of pure strange ( $s$ ) or anti-strange ( $\bar{s}$ ) constituent quarks and of the  $\phi$  meson, consisting of one  $s$  and one  $\bar{s}$  constituent quark.

Figure 2 shows the  $v_2$  as a function of  $p_T$  for  $\pi$ ,  $p$ ,  $\phi$  and  $\Omega$  for 0-80% centrality in Au + Au collisions at  $\sqrt{s_{NN}} = 200$  GeV. Here  $\phi$  and  $\Omega$   $v_2$  are corrected for the event bias mentioned earlier. Panel (a) of Figure 2 shows a comparison between  $v_2$  of  $\pi$  and  $p$ , consisting of up ( $u$ ) and down ( $d$ ) light quarks, and panel (b) shows a comparison of  $v_2$  of  $\phi$  and  $\Omega$  containing heavier  $s$  quarks. The  $v_2$  of  $\phi$  and  $\Omega$  are mass ordered at low  $p_T$  and a baryon-meson separation is observed at intermediate  $p_T$ . It is clear from Figure 2 that the  $v_2(p_T)$  of hadrons consisting only of strange quarks ( $\phi$  and  $\Omega$ ) is similar to that of  $\pi$  and  $p$ . However, unlike  $\pi$  and  $p$ , the  $\phi$  and  $\Omega$  do not participate strongly in the hadronic interactions, which suggests that the major part of collectivity is developed during the partonic phase in Au + Au collisions at  $\sqrt{s_{NN}} = 200$  GeV.

We now compare our results for NCQ scaling for different collision centrality classes to see how the partonic collectivity changes with system size. Figure 3 shows the  $v_2$  scaled by number of constituent quarks ( $n_q$ ) as a function of  $p_T/n_q$  and  $(m_T - m_0)/n_q$  for identified hadrons from Au + Au collisions at  $\sqrt{s_{NN}} = 200$  GeV for 0-30% and 30-80% centrality, where  $m_T$  and  $m_0$  are the transverse mass and rest mass of hadron, respectively. Here,  $\phi$ ,  $\Xi$  and  $\Omega$   $v_2$  are corrected for the event bias mentioned above. To quantify the deviation from NCQ scaling, we fit the  $K_S^0$   $v_2$  with a third-order



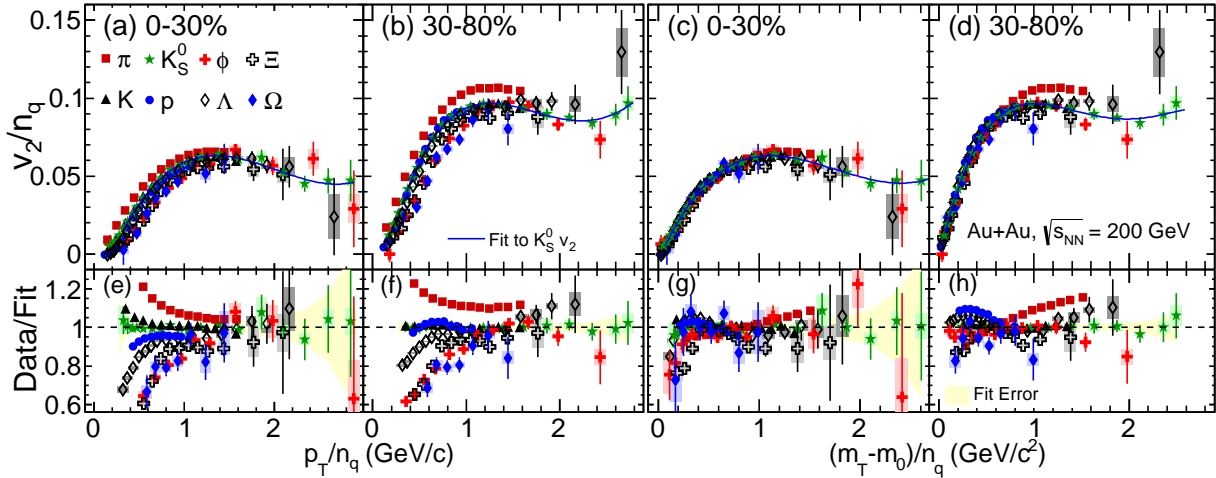


FIG. 3. (Color online) The  $v_2$  scaled by number of constituent quarks ( $n_q$ ) as a function of  $p_T/n_q$  and  $(m_T - m_0)/n_q$  for identified hadrons from Au + Au collisions at  $\sqrt{s_{NN}} = 200$  GeV. Ratios with respect to a polynomial fit to the  $K_S^0 v_2$  are shown in the corresponding lower panels. Vertical lines are statistical uncertainties and shaded boxes are systematic uncertainties.

polynomial function. We then take the ratio of  $v_2$  for the other measured hadrons to the  $K_S^0$  fit. The ratios are shown in the lower panels of Figure 3. Table I shows the deviations of  $\phi$ ,  $\Lambda$ ,  $\Xi$  and  $\Omega$   $v_2$  from the  $K_S^0$  fit line in the range  $(m_T - m_0)/n_q > 0.8$  GeV/ $c^2$ .

For both 0-30% and 30-80% centralities, the scaling

TABLE I. Deviation from the  $K_S^0$  fit line in the range  $(m_T - m_0)/n_q > 0.8$  GeV/ $c^2$  for 0-30% and 30-80% centrality.

Particle	Deviation	
	0-30% centrality	30-80% centrality
$\phi$	$2.7 \pm 2.6(\text{stat.}) \pm 1.8(\text{sys.})\%$	$1.2 \pm 1.3(\text{stat.}) \pm 0.6(\text{sys.})\%$
$\Lambda$	$4.3 \pm 0.8(\text{stat.}) \pm 0.2(\text{sys.})\%$	$1.5 \pm 0.7(\text{stat.}) \pm 0.2(\text{sys.})\%$
$\Xi$	$11.3 \pm 2.3(\text{stat.}) \pm 1.4(\text{sys.})\%$	$8.5 \pm 2.0(\text{stat.}) \pm 0.5(\text{sys.})\%$
$\Omega$	$10.1 \pm 8.4(\text{stat.}) \pm 5.3(\text{sys.})\%$	$7.0 \pm 6.0(\text{stat.}) \pm 1.5(\text{sys.})\%$

holds approximately within 10%, excluding pions. The deviation of pions could be due the effect of resonance decay and non-flow correlations [34]. We have seen similar order ( $\sim 10\%$ ) of deviation if we use  $p_T/n_q$  scaling as a reference. The maximum deviation from NCQ scaling is  $\sim 20\%$  at  $\sqrt{s_{NN}} = 2.76$  TeV as observed by ALICE experiment [35]. Therefore, at top RHIC energy, NCQ scaling holds better than LHC energy. The observed difference between the charged kaon and  $K_S^0 v_2$  at low  $p_T$  is due to differences in the pile-up protection conditions used in collecting the different data sets. The difference is taken to be an additional contribution to the systematic error on  $K_S^0 v_2$ .

Hydrodynamical model calculations predict that  $v_2$  as a function of  $p_T$  follows mass ordering, where the  $v_2$  of heavier hadrons is lower than that of lighter hadrons and vice-versa [3, 36, 37]. Mass ordering is indeed observed in the identified hadron  $v_2$  measured in the low  $p_T$  region ( $p_T \leq 1.5$  GeV/ $c$ ) [28]. Recent phenomenological

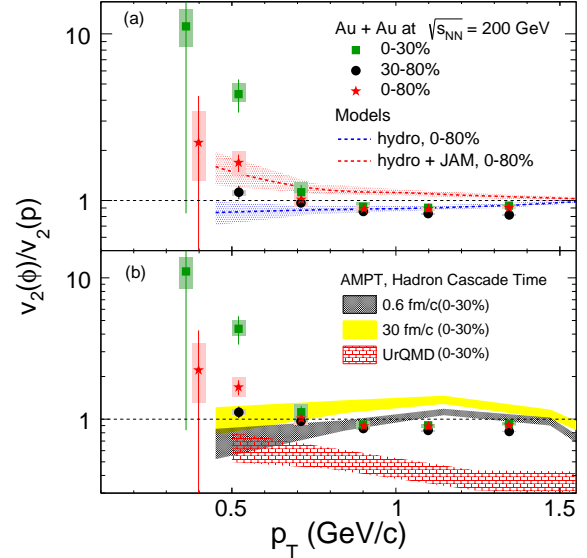


FIG. 4. (Color online)  $v_2(\phi)/v_2(p)$  ratio as function of  $p_T$  for 0-30%, 30-80% and 0-80% centrality in Au + Au collisions at  $\sqrt{s_{NN}} = 200$  GeV. Shaded boxes are the systematic uncertainties and vertical lines are the statistical uncertainties. The first data point of 0-80% centrality is shifted towards right by 400 MeV/ $c$ . The bands in panel (a) and (b) represent the hydro model [8] and transport model calculations for  $v_2(\phi)/v_2(p)$ , respectively.

calculations, based on ideal hydrodynamics together with a hadron cascade (JAM), show that the mass ordering of  $v_2$  could be broken between  $\phi$  mesons and protons at low  $p_T$  ( $p_T < 1.5$  GeV/ $c$ ) [7, 8]. The broken mass ordering is thought to be due to late stage hadronic re-scattering effects on the proton  $v_2$ , since the model calculations assume a low hadronic cross-section for the

$\phi$  but a large hadronic cross-section for the proton. The ratios of  $\phi$   $v_2$  and proton  $v_2$  are shown in Figure 4. The ratios are larger than unity at  $p_T \sim 0.5$  GeV/c for 0-30% centrality showing an indication of breakdown of the expected mass ordering in that momentum range. This could be due to a large effect of hadronic re-scattering on the proton  $v_2$ , indicated by the shaded red band in panel (a) of Figure 4. We have also considered the effect of the momentum resolution and energy loss of the TPC as well as decay (feed-down) effects on the proton  $v_2$ . Our study, based on the UrQMD framework, indicates that the momentum resolution and decay effects on the ratio of  $v_2(\phi)$  to  $v_2(p)$  in the measured momentum region are negligible. The break down of mass ordering of  $v_2$  is more pronounced in 0-30% than in 30-80% centrality. For example, the ratio  $v_2(\phi)/v_2(p)$  is  $4.35 \pm 0.98 \pm_{0.45}^{0.66}$  at  $p_T = 0.52$  GeV/c in 0-30%, while it is  $1.12 \pm 0.10 \pm_{0.053}^{0.047}$  in 30-80%. In the central events, both hadronic and partonic interactions are larger than in peripheral events. Therefore, the combined effects of large partonic collectivity on the  $\phi$   $v_2$  and significant late stage hadronic interactions on the proton  $v_2$  produce a greater breakdown of mass ordering in the 0-30% centrality data than in the 30-80% [15]. This observation indirectly supports the idea of a small hadronic interaction cross-section for the  $\phi$  meson. We have also studied the ratio of  $\phi$   $v_2$  to proton  $v_2$  using the transport models AMPT [38] and UrQMD [39]. The  $v_2(\phi)/v_2(p)$  ratio for 0-30% centrality from AMPT and UrQMD model are shown in Figure 4 (panel b). The black shaded band is from AMPT with a hadronic cascade time of 0.6 fm/c while the yellow band is for a hadronic cascade time of 30 fm/c. It is clear from Figure 4 (panel b) that with increasing hadronic cascade time (and therefore more hadronic re-scattering), the  $v_2(\phi)/v_2(p)$  ratio increases. This is attributed to a decrease in the proton  $v_2$  due to an increase in hadronic re-scattering

while the  $\phi$ -meson  $v_2$  remains unaffected [15]. The ratios from UrQMD are shown as a red shaded band which is much smaller than unity. The UrQMD model lacks partonic collectivity and therefore does not fully develop the  $\phi$ -meson  $v_2$ .

In summary, we have reported high-statistics elliptic flow measurements for multi-strange hadrons ( $\Xi$  and  $\Omega$ ) and  $\phi$  meson with other light and strange hadrons ( $\pi$ ,  $K$ ,  $K_S^0$ ,  $p$  and  $\Lambda$ ) in Au + Au collisions at  $\sqrt{s_{NN}} = 200$  GeV for different centralities. The  $p_T$  dependence of  $\phi$  and  $\Omega$   $v_2$  is observed to be similar to that of  $\pi$  and  $p$ , indicating that a large amount of collectivity is developed in the initial partonic phase for light and strange hadrons. NCQ scaling holds within the statistical uncertainty for both 0-30% and 30-80% centralities, suggesting collective motion of quarks prior to hadronization. The comparison between the  $\phi$  and  $p$   $v_2$  shows that at low  $p_T$ , there is a possible violation of hydrodynamics-inspired mass ordering between  $\phi$  and  $p$ . Model calculations suggest that the  $p_T$  dependence of  $v_2(\phi)/v_2(p)$  can be qualitatively explained by the effect of late-stage hadronic re-scattering on the proton  $v_2$  [7, 8].

We thank the RHIC Operations Group and RCF at BNL, the NERSC Center at LBNL, the KISTI Center in Korea, and the Open Science Grid consortium for providing resources and support. This work was supported in part by the Office of Nuclear Physics within the U.S. DOE Office of Science, the U.S. NSF, the Ministry of Education and Science of the Russian Federation, NNSFC, CAS, MoST and MoE of China, the Korean Research Foundation, GA and MSMT of the Czech Republic, FIAS of Germany, DAE, DST, and UGC of India, the National Science Centre of Poland, National Research Foundation, the Ministry of Science, Education and Sports of the Republic of Croatia, and RosAtom of Russia.

- 
- [1] QCD and instantons at finite temperature. D. J. Gross, R. D. Pisarski, and L. G. Yaffe, *Rev. Mod. Phys.* **53**, 43 (1981).
- [2] Anisotropy as a signature of transverse collective flow. J. Y. Ollitrault, *Phys. Rev.* **D 46**, 229 (1992).
- [3] Radial and elliptic flow at RHIC: further predictions. P. Huovinen *et al.*, *Phys. Lett.* **B 503**, 58 (2001).
- [4] Azimuthal anisotropy in Au+Au collisions at  $\sqrt{s_{NN}} = 200$  GeV. J. Adams *et al.*, *Phys. Rev.* **C 72**, 014904 (2005).
- [5] Mass, quark-number, and  $\sqrt{s_{NN}}$  dependence of the second and fourth flow harmonics in ultra-relativistic nucleus-nucleus collisions. B. I. Abelev *et al.*, *Phys. Rev.* **C 75**, 054906 (2007).
- [6] Charged and strange hadron elliptic flow in Cu+Cu collisions at  $\sqrt{s_{NN}} = 62.4$  and 200 GeV. B. I. Abelev *et al.*, *Phys. Rev.* **C 81**, 044902 (2010).
- [7] Mass ordering of differential elliptic flow and its violation for  $\phi$  mesons. T. Hirano *et al.*, *Phys. Rev.* **C 77**, 044909 (2008).
- [8] Hadronic rescattering effects on multi-strange hadrons in high-energy nuclear collisions. S. Takeuchi *et al.*, arXiv:1505.05961.
- [9]  $\phi$ -Meson Production as a Probe of the Quark-Gluon Plasma. A. Shor, *Phys. Rev. Lett.* **54**, 1122 (1985).
- [10] Experimental and Theoretical Challenges in the Search for the Quark Gluon Plasma: The STAR Collaboration's Critical Assessment of the Evidence from RHIC Collisions. J. Adams *et al.*, *Nucl. Phys.* **A 757** 102-183 (2005).
- [11] Evidence of Early Multistrange Hadron Freeze-Out in High Energy Nuclear Collisions. H. van Hecke, H. Sorge and N. Xu, *Phys. Rev. Lett.* **81**, 5764 (1998).
- [12] Probe the QCD phase diagram with  $\phi$ -mesons in high energy nuclear collisions. B. Mohanty and N. Xu, *J. Phys.* **G 36**, 064022 (2009).

- [13] Parton distributions at hadronization from bulk dense matter produced in Au+Au collisions at  $\sqrt{s_{NN}} = 200$ . J. H. Chen *et al.*, Phys. Rev. **C 78**, 034907 (2008).
- [14] Elliptic flow of  $\phi$  mesons and strange quark collectivity. J. H. Chen *et al.*, Phys. Rev. **C 74**, 064902 (2006).
- [15] Elliptic flow of  $\phi$  mesons as a sensitive probe for the onset of the deconfinement transition in high energy heavy-ion collisions. M. Nasim, B. Mohanty and N. Xu, Phys. Rev. **C 87**, 014903 (2013).
- [16] Spectra and elliptic flow for  $\Lambda$ ,  $\Xi$ , and  $\Omega$  in 200 A GeV Au+Au collisions. X. Zhu and H. Song, arXiv:1509.05482.
- [17] Multistrange Baryon Elliptic Flow in Au+Au Collisions at  $\sqrt{s_{NN}} = 200$  GeV. J. Adams *et al.*, Phys. Rev. Lett. **95**, 122301 (2005).
- [18] Identified particle production, azimuthal anisotropy, and interferometry measurements in Au+Au collisions at  $\sqrt{s_{NN}} = 9.2$  GeV. B. I. Abelev *et al.*, Phys. Rev. **C 81**, 024911 (2010).
- [19] Quantum Optics and Heavy Ion Physics. R. J. Glauber, Nucl. Phys **A 774**, 3 (2006).
- [20] Inclusive charged hadron elliptic flow in Au + Au collisions at  $\sqrt{s_{NN}} = 7.7 - 39$  GeV. L. Adamczyk *et al.*, Phys. Rev. **C 86**, 054908 (2012).
- [21] Azimuthal Anisotropy of  $K_S^0$  and  $\Lambda + \bar{\Lambda}$  Production at Midrapidity from Au+Au Collisions at  $\sqrt{s_{NN}} = 130$  GeV. C. Adler *et al.*, Phys. Rev. Lett. **89**, 132301 (2002).
- [22] Particle-Type Dependence of Azimuthal Anisotropy and Nuclear Modification of Particle Production in Au+Au Collisions at  $\sqrt{s_{NN}} = 200$  GeV. J. Adams *et al.*, Phys. Rev. Lett. **92**, 052302 (2004).
- [23] Methods for analyzing anisotropic flow in relativistic nuclear collisions. A. M. Poskanzer and S. A. Voloshin, Phys. Rev. **C 58**, 1671 (1998).
- [24] Azimuthally sensitive correlations in nucleus-nucleus collisions. N. Borghini and J.-Y. Ollitrault, Phys. Rev. **C 70**, 064905 (2004).
- [25] Event plane resolution correction for azimuthal anisotropy in wide centrality bins. H. Masui and A. Schmah, arXiv:1212.3650.
- [26] Systematic study of the elliptic flow parameter using a transport approach. M. Nasim and B. Mohanty, Int. J. Mod. Phys. **E 24**, 1550027 (2015).
- [27] Color Glass Condensate and Glasma. F. Gelis, Int. J. Mod. Phys. **A 28**, 1330001 (2013).
- [28] Centrality dependence of charged hadron and strange hadron elliptic flow from  $\sqrt{s_{NN}} = 200$  GeV Au+Au collisions. B. I. Abelev *et al.*, Phys. Rev. **C 77**, 054901 (2008).
- [29] Partonic Flow and  $\phi$ -Meson Production in Au+Au Collisions at  $\sqrt{s_{NN}} = 200$  GeV. B. I. Abelev *et al.*, Phys. Rev. Lett. **99**, 112301 (2007).
- [30] Elliptic Flow at Large Transverse Momenta from Quark Coalescence. D. Molnar and S. A. Voloshin, Phys. Rev. Lett. **91**, 092301 (2003).
- [31] Hadronization in Heavy-Ion Collisions: Recombination and Fragmentation of Partons. R. J. Fries *et al.*, Phys. Rev. Lett. **90**, 202303 (2003).
- [32] Initial fluctuation effect on harmonic flows in high-energy heavy-ion collisions. L. X. Han *et al.*, Phys. Rev. **C 84**, 064907 (2011).
- [33] Constituent quark scaling violation due to baryon number transport. J. C. Dunlop, M. A. Lisa, and P. Sorensen, Phys. Rev. **C 84**, 044914 (2011).
- [34] Resonance decay effects on anisotropy parameters. X. Dong *et al.*, Phys. Lett. **B 597**, 328 (2004) and Quark Gluon Plasma 4, edited by R.C. Hwa and X.N. Wang, page 339.
- [35] Elliptic flow of identified hadrons in Pb-Pb collisions at  $\sqrt{s_{NN}} = 2.76$  TeV. B. B. Abelev *et al.*, (ALICE Collaboration) JHEP 1506, 190 (2015).
- [36] Elliptic flow of multi-strange particles: fragmentation, recombination and hydrodynamics. C. Nonaka, R. J. Fries, and S. A. Bass, Phys. Lett. **B 583**, 73 (2004).
- [37] Interplay between soft and hard hadronic components for identified hadrons in relativistic heavy ion collisions. T. Hirano and Y. Nara, Phys. Rev. **C 69**, 034908 (2004).
- [38] Multiphase transport model for relativistic heavy ion collisions. Z.-W. Lin *et al.*, Phys. Rev. **C 72**, 064901 (2005).
- [39] Microscopic Models for Ultrarelativistic Heavy Ion Collisions. S. A. Bass *et al.*, Prog. Part. Nucl. Phys. **41**, 255 (1998).